International Journal of Thermal Sciences xxx (xxxx) xxx–xxx

Contents lists available at ScienceDirect

International Journal of Thermal Sciences

journal homepage: www.elsevier.com/locate/ijts

Numerical investigation of the effects of geometric structure of microchannel heat sink on flow characteristics and heat transfer performance

Ergin Bayrak[a,*], Ali Bahadır Olcay[b], Mustafa Fazıl Serincan[c]

[a] Alanya Alaaddin Keykubat University, Department of Air Conditioning and Refrigeration Technology, 07425, Alanya, Antalya, Turkey
[b] Yeditepe University, Department of Mechanical Engineering, 34755, Atasehir, Istanbul, Turkey
[c] Gebze Technical University, Department of Mechanical Engineering, 41400, Kocaeli, Turkey

ARTICLE INFO

Keywords:
Microchannel heat sink
Heat transfer enhancement
Cavity and rib
Temperature distribution on baseline
Thermal management of lithium-ion batteries

ABSTRACT

A numerical study was performed to investigate the thermal-hydraulic performance of different microchannel heat sink (MCHS) designs for cooling channels in a lithium-ion battery including various geometric modifications. Comparative analysis was performed to determine which design is the best in terms of the heat transfer, the pressure drop, the overall performance and the temperature distribution on the baseline wall. It was observed that local modifications in channels can ensure suitable fluid mixing between core flow and near wall regions; therefore this situation enhances heat transfer performance considerably compared to MCHS with no cavity and rib (MC-NCR). However, the vortices obviously occurred in cavities. Although this phenomenon was helpful for the symmetrical cavity and rib (MC-SCR) in terms of heat transfer enhancement, it was opposite for the asymmetrical cavity and rib (MC-ACR) due to intensive recirculation zones. In addition, the large vortex bubbles especially seen after the last cavity or rib cause pick temperatures because this trapped flow could not be surpassed and carried. Results indicate that as the MC-SCR shows the best thermal performance owing to dominant jetting and throttling effect and convenient longitudinal and transverse vortices, asymmetrical cavity (MC-AC) is the best uniform temperature distribution on baseline wall.

1. Introduction

Recently there has been a significant demand to design and produce high performance electronic devices in small and compact sizes. Reduction in the size of electronic components seems to be favorable; however, it comes with thermal management concerns as the necessity to remove large heat rates from constrained spaces arises with these devices. Thermal management in lithium-ion battery packs possesses similar challenges. Utilization of the batteries in electric vehicles or other mobile applications requires large heat rejection rates per volume with cooling system components carrying overall weight and volume as small as possible.

Traditional air convection cooling methods can no longer satisfy the requirement of cooling demand for the high heat generation rate in small spaces. Instead, liquid cooling is preferred over air due to higher heat transfer coefficients and specific heat capacity [1]. On the other hand, microchannel heat sink (MCHS) is a promising cooling method in the electromechanical industry because these heat sinks with high degree of integration can remove heat from a surface at higher rates, which can reach 790 W/cm^2, owing to large surface area to volume ratios [2]. Although this method ensures significant heat transfer enhancement, it yields to additional pumping power costs due to pressure drop increase in microchannels. Thus, the MCHS systems should be evaluated and optimized considering both heat transfer and fluid flow characteristics through channels.

The studies performed for MCHS systems can be generally classified as active, passive and compound heat transfer enhancement methods. Typically, the passive method is preferred over active one since this method does not require any external power and utilizes surface modification by joining inserts into the tubes. When the passive heat transfer enhancement methods are considered in detail, it is noted that a large number of studies show the use of passive heat transfer enhancement methods to produce more efficient and compact electronic devices.

The MCHSs possessing corrugated configuration including wavy, zigzag and convergent-divergent sections has a great advantage for

* Corresponding author.
E-mail address: ergin.bayrak@alanya.edu.tr (E. Bayrak).

https://doi.org/10.1016/j.ijthermalsci.2018.08.030
Received 25 February 2018; Received in revised form 8 August 2018; Accepted 16 August 2018

micro-cooling applications because it ensures high flow mixing between warmer and colder fluid streams. This can be actually achieved when a surface modification is employed on a base wall of the MCHS system or a flow disruption is induced in a microchannel yielding higher overall thermal performance [3–12]. Wan et al. [4] performed a comparative study between half-corrugated and flat microchannel. They pointed out that wave amplitude can be neglected for their specific flow region and geometrical specifications as the wave length has significant impact on a pressure drop. Furthermore, they specified that half-corrugated MCHSs have a better overall thermal performance than other corrugated MCHSs. The study performed by Aliabadi et al. [5] showed the effect of a sinusoidal wave length and amplitude on cooling performance for the Reynolds number of 60–4000. They concluded that the heat transfer coefficient enhanced nearly 200% for a specific wave length and amplitude. Different corrugated geometries of MCHS including triangular, trapezoidal and sinusoidal were also investigated and compared with straight MCHS [6]. It was reported that the MCHS geometry with sinusoidal corrugation shape for a specific corrugation length and amplitude illustrates the best performance. Moreover, they concluded that decrease in corrugation length and increase in corrugation amplitude contributed to the enhancement of the Nusselt number and pumping power for all cases. Periodic flow field, a periodically repeated flow condition, in a periodic zigzag channel was investigated by Zheng et al. [8] and [13]. The periodic flow field in periodic zigzag channel was observed for $Re < 200$ while this periodic flow was no longer present for $Re > 400$ due to chaotic advection and strong Dean vortices [13]. It was also noted that transition of flow from steady to unsteady flow occurs at about $Re = 215$ in the zigzag channel and this situation is much lower than predicted numerical results [8]. Furthermore, they speculated that early transition can be triggered by small inlet disturbances in the experiments. The numerical optimization study was carried out by Rostami et al. [9] to determine optimum wavy microchannel geometry ensuring maximum Nusselt number. They emphasized that there is optimum wave geometry depending on the presence of the recirculation zones and secondary flows, which can be defined as fluid motion, which is perpendicular to the main flow direction, and their dependence on the Reynolds number and geometrical parameters.

Moreover, Lu et al. [11] carried out a study to thermal-fluid characteristic of wavy microchannel heat sink with porous fin. They stated that the heat transfer performance improved depending on combination of enhanced coolant mixing, prolonged flow route and forced permeation by the jet-like impingement. The other study performed by Lin et al. [12] investigated different wavelength and amplitude and theirs effects on heat transfer performance. They have concluded that decreased wave length or increased amplitude ensures lower thermal resistance and smaller temperature difference on the bottom wall. Also, they have specified that the optimum design of wave length and amplitude difference between two adjacent wavy channels ensure the best heat transfer performance.

Another mechanism used to enhance heat transfer performance is the use of cavity in a microchannel owing to its ability of flow disruption, which promotes flow instabilities and increased flow mixing. The proper design of this type of microchannel ensures low pressure drop and high thermal performance when compared to a straight microchannel. Parametric numerical studies were performed to examine the flow and heat transfer in a microchannel with dimples [14–17]. It was realized that existence of a dimple in the channel can result in a transverse convection and this can be very important in terms of convection heat transfer enhancement. Ahmed E. and Ahmed M [16]. conducted a numerical study investigating the effect of the different geometry variables and the Reynolds number. They obtained the optimum groove tip length ratio, groove depth ratio, groove pitch ratio, groove orientation ratio and Reynolds number. The remarkable point of this study is that the orientation ratio of the groove showed the optimum thermal performance for symmetrical grooves (orientation ratio of groove was 0.00). Thermal-hydraulic performance of reentrant cavity used in microchannel heat sink was investigated by Xia et al. [17]. They stated that the significant heat transfer enhancement results from the increased heat transfer area, redeveloping of boundary layer, jet and throttling effects and slipping over the reentrant cavities.

Another flow disruption method is the use of a rib in MCHS. A rib has the ability to interrupt and redevelop boundary layers and ensure forming vortices; therefore, causing increase of flow mixing in a channel. Zheng et al. [18] conducted a numerical study investigating a discrete inclined rib in a tube. They emphasized that inducing longitudinal swirl flow ensures suitable fluid mixing between core flow and near wall region; as a result, a considerable enhancement of heat transfer performance was documented. Xia et al. [19] investigated the thermal-hydraulic characteristic of a circular, square and diamond pin fin in a microchannel. It was concluded that the diamond pin fin ensures the best heat transfer enhancement because the vortices were easily involved in the main flow and they observed a high vortex intensity behind the fin. The study investigating fluid flow and heat transfer in a microchannel with various longitudinal vortex generators was performed by Chen et al. [20]. It was concluded that the critical Reynolds number was lowered below 1000 with the help of a vortex generator.

Another important flow disruption method is the use of rib and cavity combination together. There are many advantages of this method since the presence of jetting and throttling can increase the flow mixing because of intensive vortices and ensuring a larger flow area in the channel [21–26]. Ghani et al. [21] showed that the use of rib and cavity combination in the flow considerably augments overall performance in MCHS. Furthermore, it reduces the effect of stagnation zones and promotes disturbances. Li et al. [23] stated that this type of MCHS shows more uniform and lower temperature at the bottom surface of MCHS when compared to MCHS without cavity and rib. Zhai et al. [24] performed an experimental study investigating the hydrodynamics of MCHS with cavity and rib. Accordingly, the vortices formed in cavities and ribs intensified the flow turbulence with the increase of Reynolds number while the vortices in cavities were not observed at low Reynolds numbers.

MCHS with secondary channel or a combination of secondary channel and rib is the other important enhancement method used by researchers. Specifically, Ghani et al. [27] studied the combined effect of secondary flow and rib and they concluded that use of this technique contributes about 50% reduction in pressure drop due to the ribs existence. Another study performed by Kuppusamy et al. [28] only investigated the effect of secondary flow in MCHS. They found that the overall performance with optimum geometry increased by 146% and thermal resistance reduced to 76.8% when compared with simple MCHS. In addition, they highlighted that more fluid diversion into the secondary passage ensures forming of vortices in secondary passage, redevelopment of boundary layer and larger heat transfer area. Lastly, offset strip fin is another enhancement method. In this method, flow moved in short passages and then encountered the offsetting fins which split the flow streams and deviated their direction to move around the fins in this method [29]. Yu et al. [30] presented a study investigating MCHS with a Piranha Pin fin. This design disturbed the velocity field and ensured separation and mixing causing heat transfer enhancement. Furthermore, they specified that fluid extraction results in a considerable augmentation of the Nusselt number while reducing the pressure drop.

Beside the surface modification studies, there are some optimization studies considering some geometric parameters in MCHS. Wang et al. [31] obtained optimal designs of nanofluid-cooled MCHS by optimizing channel number, channel aspect ratio and width ratio of channel to pitch at fixed and various constraint conditions. Another study carried out by Lin et al. [32] proposed a design strategy for double-layer MCHS. It investigated six design variables and optimized these variables by searching for a minimum of global thermal resistance at fixed and

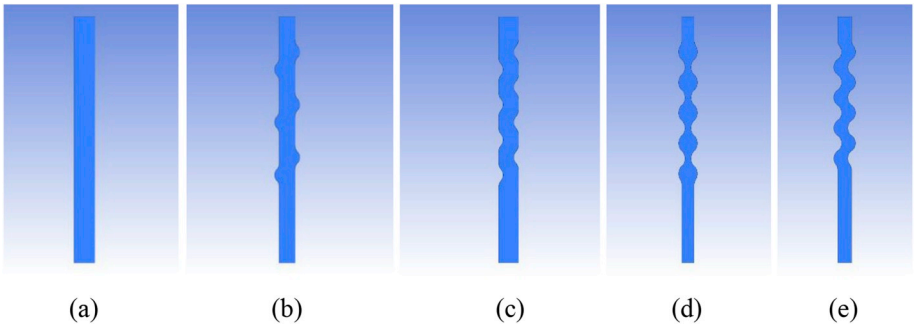

Fig. 1. Geometric models: (a) a microchannel with no cavity and rib (MC-NCR); (b) a microchannel with asymmetric cavity (MC-AC) (c) a microchannel with asymmetric rib (MC-AR) (d) a microchannel with symmetric cavity and rib (MC-SCR) (e) a microchannel with asymmetric cavity and rib (MC-ACR).

various constraint conditions. Another study on optimization of double-layered MCHS with truncated top channels was performed by Leng et al. [33]. They concluded that the truncated MCHS was highly recommended for larger channel number, smaller channel to pitch width ratio, smaller total pumping power to enhance performance.

Previous literature indicates that most of the studies on MCHSs were conducted by considering only one enhancement method instead of a combined method or ignored the temperature uniformity and pick temperatures forming on the baseline wall. However, the present numerical study revisited surface modification methods and focused on the investigation of thermal-hydraulic performance and temperature uniformity on the MCHSs. Since temperature gradient in an electronic device can undermine the performance of the device and even shorten the life of a device, it is aimed to evaluate temperature uniformity and identify any temperature picks for the studied cases to eliminate thermal runaway. In the current work, the studies performed was classified as corrugated MCHS, cavities in MCHS, rib in MCHS, cavity and rib together in MCHS, secondary channel in MCHS, offset strip fin in MCHS and interrupted wall channel. Particularly, MCHSs possess various cavity, rib or combination of theirs used in a cooling plate of electrochemical battery. Moreover, the mechanism between of fluid flow and heat transfer enhancement has been evaluated in detail and revealed the importance of surface modification on overall performance.

2. The design of a microchannel heat sink

In this study, different types of microchannel designs are used and they are illustrated in Fig. 1. These microchannels are named: microchannel with no cavity and rib (MC-NCR), microchannel with asymmetric cavity (MC-AC), microchannel with asymmetric rib (MC-AR), microchannel with symmetric cavity and rib (MC-SCR) and microchannel with asymmetric cavity and rib (MC-ACR). Table 1 provides geometrical details of each microchannel while Fig. 2 shows the representation of dimensional parameters such as channel width and length, wave length and amplitude. Meanwhile, channel width and length and wave amplitude are kept the same for all studied cases; however, wave length is allowed to be different.

3. Numerical method

The computational fluid dynamic (CFD) software ANSYS FLUENT 19.0 was used to solve the three-dimensional heat transfer and fluid flow equations in the computational domain. Fluid flow in MCHS was assumed to be laminar, steady state, incompressible and Newtonian; furthermore, viscous dissipation, gravitational force and radiation heat transfer effects were neglected. Moreover, the Knudsen number (Kn) was calculated to be less than 10^{-3} ensuring that the fluid flow to be continuum flow and Navier-Stokes equations with classical no-slip boundary conditions were applicable for this study [34].

3.1. Governing equations

The governing equations of incompressible flow in a microchannel are provided below in detail. Continuity, momentum and energy equations were given in equations (1), (2) to (4) and (5), respectively.

$$\rho\left(\frac{\partial u}{\partial x}+\frac{\partial v}{\partial y}+\frac{\partial w}{\partial z}\right)=0 \tag{1}$$

$$\rho\left(u\frac{\partial u}{\partial x}+v\frac{\partial u}{\partial y}+w\frac{\partial u}{\partial z}\right)=\frac{\partial}{\partial x}\left(\mu\frac{\partial u}{\partial x}\right)+\frac{\partial}{\partial y}\left(\mu\frac{\partial u}{\partial y}\right)+\frac{\partial}{\partial z}\left(\mu\frac{\partial u}{\partial z}\right)-\frac{\partial P}{\partial x} \tag{2}$$

$$\rho\left(u\frac{\partial v}{\partial x}+v\frac{\partial v}{\partial y}+w\frac{\partial v}{\partial z}\right)=\frac{\partial}{\partial x}\left(\mu\frac{\partial v}{\partial x}\right)+\frac{\partial}{\partial y}\left(\mu\frac{\partial v}{\partial y}\right)+\frac{\partial}{\partial z}\left(\mu\frac{\partial v}{\partial z}\right)-\frac{\partial P}{\partial y} \tag{3}$$

$$\rho\left(u\frac{\partial w}{\partial x}+v\frac{\partial w}{\partial y}+w\frac{\partial w}{\partial z}\right)=\frac{\partial}{\partial x}\left(\mu\frac{\partial w}{\partial x}\right)+\frac{\partial}{\partial y}\left(\mu\frac{\partial w}{\partial y}\right)+\frac{\partial}{\partial z}\left(\mu\frac{\partial w}{\partial z}\right)-\frac{\partial P}{\partial z} \tag{4}$$

$$\rho\left(u\frac{\partial T}{\partial x}+v\frac{\partial T}{\partial y}+w\frac{\partial T}{\partial z}\right)=\frac{\partial}{\partial x}\left(\frac{k_f}{c_p}\frac{\partial T}{\partial x}\right)+\frac{\partial}{\partial y}\left(\frac{k_f}{c_p}\frac{\partial T}{\partial y}\right)+\frac{\partial}{\partial z}\left(\frac{k_f}{c_p}\frac{\partial T}{\partial z}\right) \tag{5}$$

where u, v, w are the velocity components in the x, y and z directions, respectively while ρ, P, μ, c_p, k_f and T are the coolant density, coolant pressure, dynamic viscosity coefficient of coolant, specific heat capacity of coolant, thermal conductivity of coolant and temperature of coolant, respectively.

Apart from the governing equations, related boundary conditions were determined as follows:

Table 1
Specifications of entire cases.

Case	Width of MCHS (W_c), mm	Height of MCHS (H_c), mm	Wave length (W_L), mm	Wave amplitude (A), mm	Hydraulic diameter (D_H), mm	Length of the MCHS (L), mm
MC-NCR	1	0.5	0	0.25	0.66	14
MC-AC	1	0.5	2	0.25	0.66	14
MC-AR	1	0.5	2	0.25	0.66	14
MC-SCR	1	0.5	1.732	0.25	0.66	14
MC-ACR	1	0.5	1.732	0.25	0.66	14

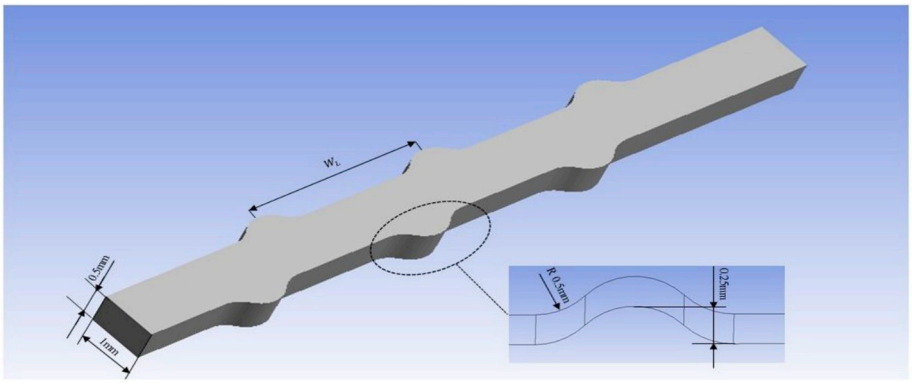

Fig. 2. Schematic representation of MCHS.

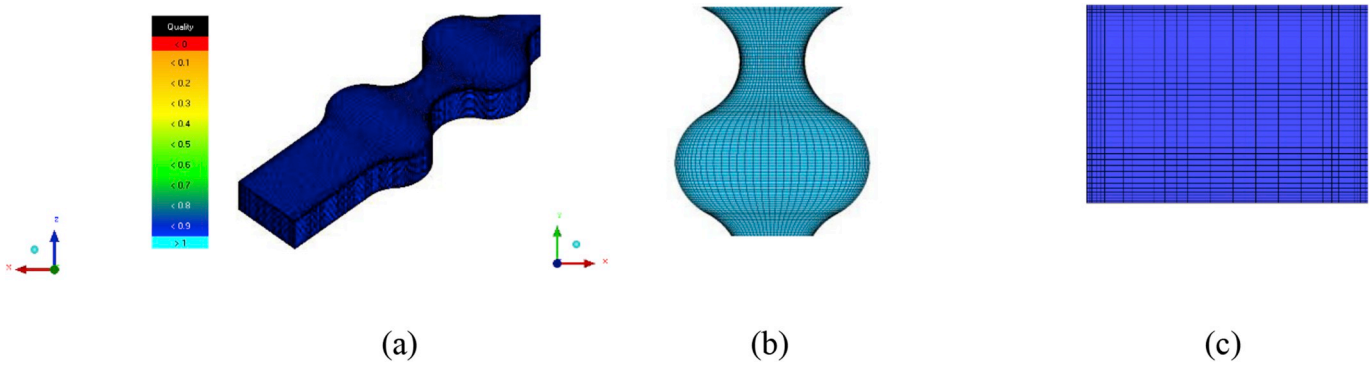

Fig. 3. Three-dimensional hexahedral mesh structure of MC-SCR and its boundary layer (a) general view (b) *x-z* cross section (c) *x-y* cross section.

Table 2
Mesh independence test for the MC-NCR.

No	*Re*	Grid Number × 10^6	ΔP (Pa)	e (%)
1	600	0.672165	1434.615	0.74
2	600	0.839865	1438.371	0.48
3	600	1.007565	1441.059	0.29
4	600	2.68593	1445.3	–

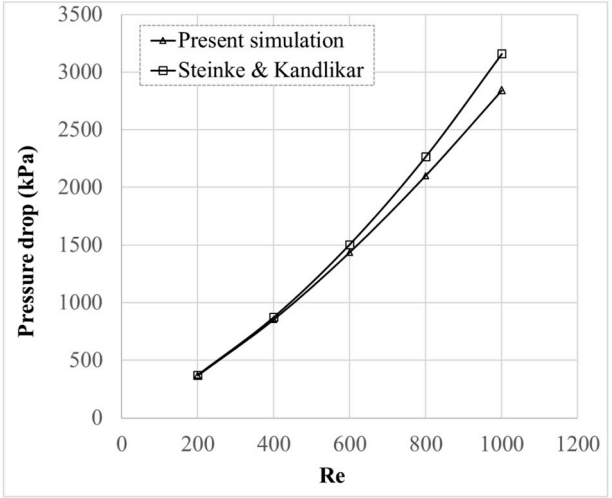

Fig. 4. The validation graphic of pressure drop versus Re.

(1) The uniform velocity and temperature were applied at the inlet of the microchannel. This implies that velocity driven flow was utilized in the present study since uniform velocity was applied for the inlet boundary condition. Therefore, the inlet velocity is in the *z* direction and its value was 0.9205 m/s, the temperature was set to 298.15 K.
(2) The relative outlet pressure was taken to be 0 Pa gage pressure at the exit of the microchannel.
(3) The constant heat flux of 30 kW/m^2 was employed to the bottom wall of a microchannel. The other walls were assumed to be adiabatic.

Lastly, water was used as a coolant in this study because of its availability, low cost and high heat capacity. The density, the dynamic viscosity and the conductivity of water were taken to be 997 kg/m^3, 0.000891 N s/m^2 and 0.607 W/m K, respectively.

3.2. Grid independence and validation

The mesh elements of the computational model were generated by the aid of ICEM CFD meshing program. As the grid type for the entire domain was set to structured uniform hexahedral elements, the mesh quality was given in detail as shown in Fig. 3. A finer mesh resolution was applied for the near wall region to capture the velocity and temperature gradients. Second-order upwind scheme was used to discretize the convection terms while the Semi-Implicit method for Pressure-Linked (SIMPLE) algorithm was used to accomplish the pressure-velocity field coupling [3,9,16,18,27,28]. Furthermore, the residual criterion was set to 10^{-4} for continuity and momentum equations while iterations continued until 10^{-6} for the energy equation.

A grid independence test was performed to obtain the most convenient mesh structure ensuring high accuracy with less computational

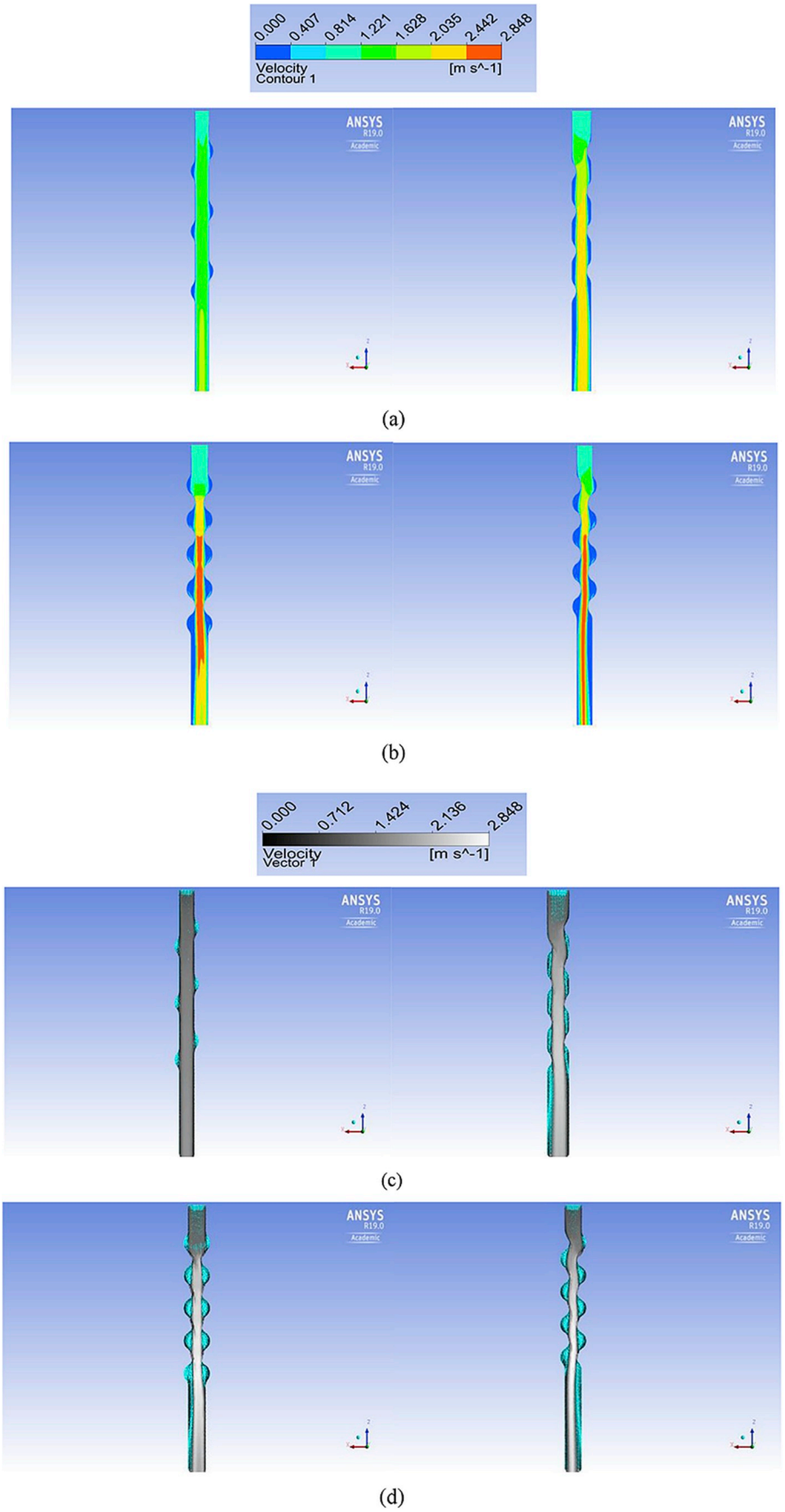

Fig. 5. Velocity contours for (a) MC-AC and MC-AR (b) MC-SCR and MC-ACR and velocity vector plots for (c) MC-AC and MC-AR (d) MC-SCR and MC-ACR.

effort. The number of mesh elements were changed from 0.672 million to 2.685 million for the Reynolds number (Re) of 600 in the test. Table 2 briefly demonstrates the relative error defined in equation (6) between the finest grid (G_1) and the other grids (G_2). It can be concluded that the computational model with 1.007 million provided a reasonable error for the pressure drop value compared to the other models with different number of elements.

$$e = |\frac{G_2 - G_1}{G_1}| \times 100 \tag{6}$$

On the other hand, the pressure drop values obtained from numerical simulations were validated with an analytical study for the MC-NCR using the correlations of Steinke & Kandlikar [27] as shown in equation (7),

$$\Delta P = \frac{2(fRe)\mu u_m L_t}{D_H^2} + \frac{\alpha(x)\rho u_m^2}{2} \tag{7}$$

where $\alpha(x)$ is defined in equation (8) below as and AR denotes the aspect ratio of microchannel.

$$\alpha(x) = 0.6796 + 1.2197(AR) + 3.3089(AR)^2 - 9.5921(AR)^3 + 8.9089(AR)^4 - 2.9959(AR)^5 \tag{8}$$

Fig. 4 shows the deviation between present simulation's findings and analytical results from Steinke & Kandlikar [34] for different Reynolds numbers. equation (7) considers developing region effects besides friction and it estimates the fully developed region to begin with a fix length. Therefore the difference could be due to the fact that Steinke and Kandlikar may be over predicting the pressure drop value at higher Reynolds number values since similar differences have been identified at some other studies [10,14]. It can be concluded that the present simulation results are in good agreement with analytical results and current CFD model with 1.007 million elements can be further used to investigate the thermal-hydraulic performance of other studied cases.

3.3. Data reduction

This section presents the expressions used in this study to identify the thermal-hydraulic characteristics of microchannel heat sinks by applying the constant heat flux from the bottom wall.

The hydraulic diameter D_H and Reynolds number Re are expressed in equations (9) and (10), respectively as:

$$D_H = \frac{2H_c W_c}{H_c + W_c} \tag{9}$$

$$Re = \frac{\rho V D_H}{\mu} \tag{10}$$

where V, H_c and W_c are mean velocity, height and width of microchannel, respectively.

The friction factor is calculated by the pressure drops:

$$f = \frac{2D_H \Delta P}{L\rho V^2} \tag{11}$$

The term of L and ΔP denote the total length of microchannel and the pressure drop across microchannel, respectively.

The average heat transfer coefficient is defined as

$$h_{avg} = \frac{qA_f}{A_c(T_{w,avg} - T_{f,avg})} \tag{12}$$

The terms of q, A_f, A_c, $T_{w,avg}$ and $T_{f,avg}$ denote the heat flux per unit area, the heated area, the convection heat transfer area, the average wall temperature and the average fluid temperature respectively. A_f and A_c were considered equal in this study; therefore, the ratio of A_f to A_c becomes 1. Average wall and fluid temperatures in the present study are calculated thru the numerical model via Ansys CFD Post.

The average Nusselt number is expressed as,

$$Nu = \frac{h_{avg} D_H}{k} \tag{13}$$

where k denotes the thermal conductivity of the cooling fluid, namely water.

The overall performance of the studied cases was evaluated using the performance factor. It is defined as the Nusselt number ratios over friction factor ratio to the power of one third [35], which can be formally written as:

$$\xi = \frac{Nu_e/Nu_0}{(f_e/f_0)^{1/3}} \tag{14}$$

where subscripts e and o are the cases that ensure the enhanced microchannel and smooth microchannel, respectively.

$$\Delta T_b = T_{max} - T_{min} \tag{15}$$

ΔT_b is defined as the temperature difference between maximum and minimum temperature on the heated surface to reflect the uniformity of temperature distribution of the MCHS [26,36]. Furthermore, the terms T_{max} and T_{min} represent the value of maximum and minimum temperatures on the heated surface.

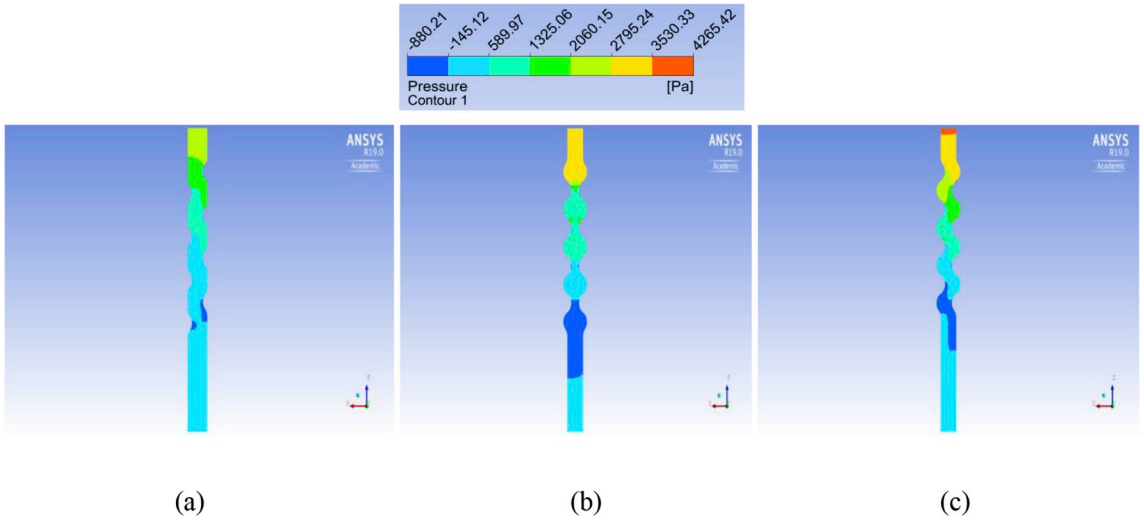

Fig. 6. Cases where negative pressure values were observed (a) MC-AR (b) MC-SCR (c) MC-ACR.

4. Results and discussion

A comparative analysis was performed in terms of heat transfer and fluid flow characteristics to evaluate the impact of different MCHS geometries. Furthermore, overall performances of MCHS geometries were determined related to fluid flow and heat transfer equations as specified in the data reduction section. The findings of the study are given in the following sections in detail.

4.1. Fluid flow characteristics

Fluid flow characteristics play an integral role in understanding physics of fluid flow in the microchannel geometries. Therefore, velocity and pressure contour plots were obtained for the computational

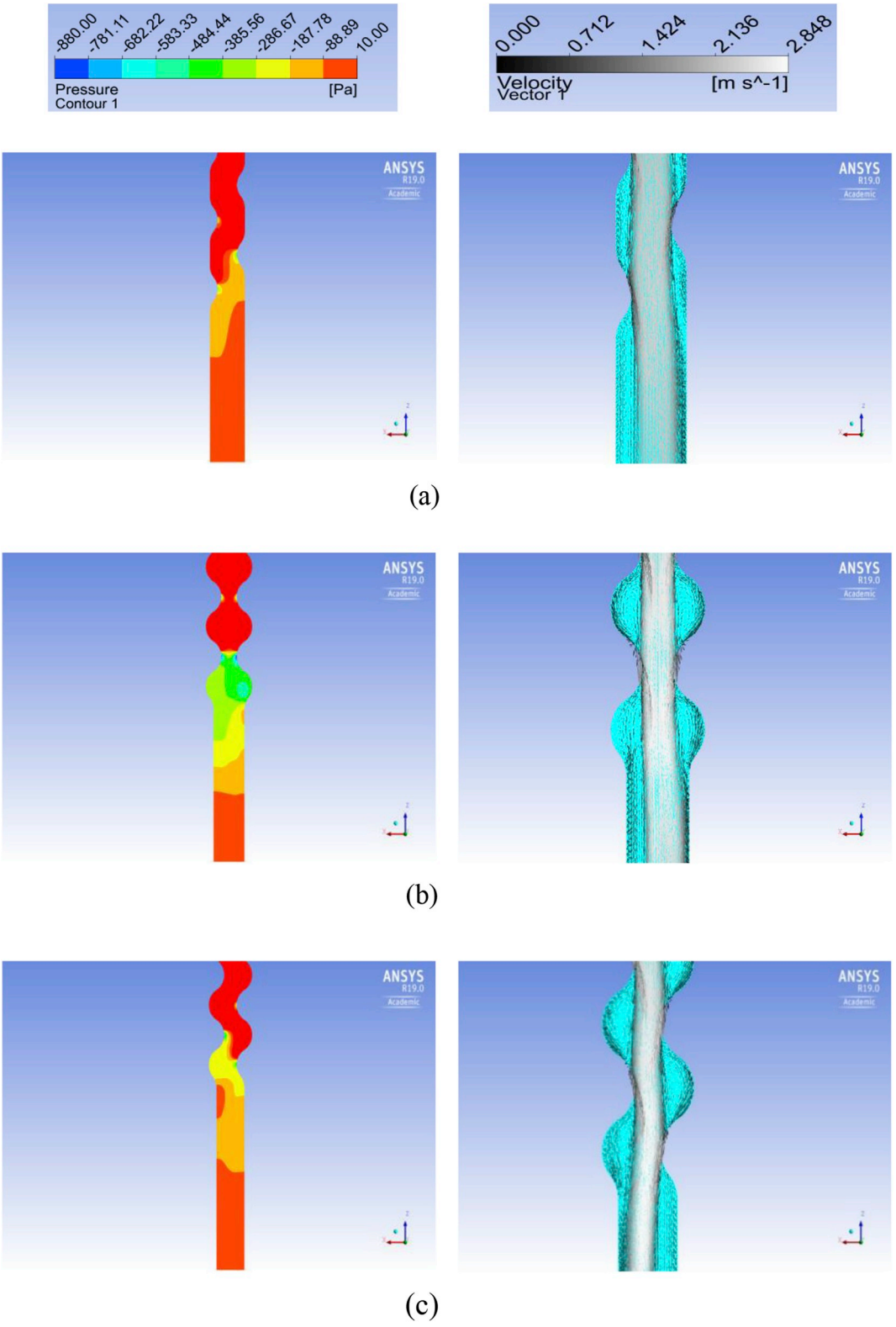

Fig. 7. The detailed view of pressure drops and velocity vectors (a) MC-AR (b) MC-SCR (c) MC-ACR.

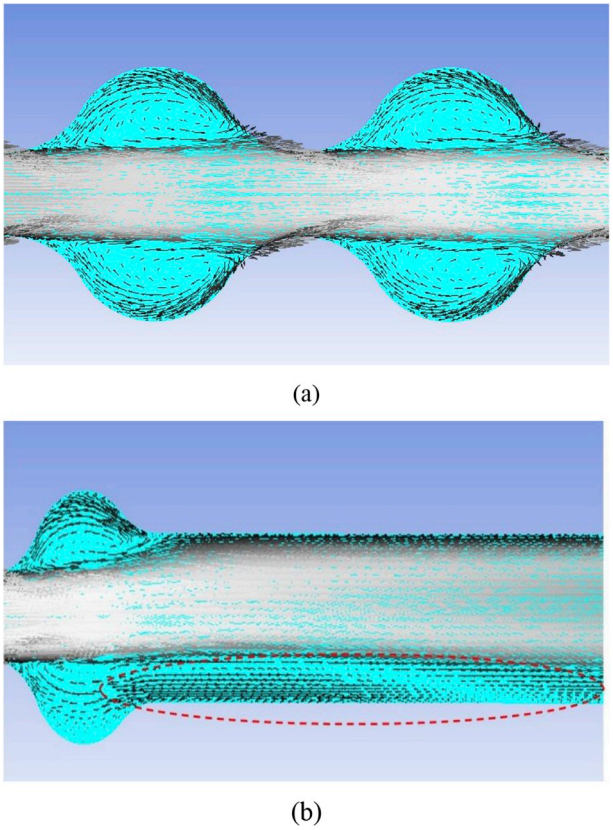

Fig. 8. (a) The formation of vortex in MC-SCR (b) the vortex bubble occurring after the last cavity in MC-SCR.

domain and demonstrated here. Fig. 5 shows velocity contour and velocity vector plots of five different microchannel geometries, namely a straight rectangular channel (i.e., MC-NCR) and channels with various corrugation shapes. It was noticed that fluid flow velocities were obtained to be very low even nearly zero at some locations inside the corrugation region implying that heat transfer due to convection may be heavily undermined. Besides, presence of corrugation affected main flow characteristics by decreasing the channel passage where fluid flow was accelerated. While higher velocities in the channel passage may imply flow regime to be in transition or in turbulent, fluid flow velocities, pressure and temperature contours do not possess any fluctuation in the present study indicating flow regime to be laminar.

When pressure variation in the rectangular channel was considered, all studied cases showed pressure drop across the channel length due to viscous effects. However, back pressure (i.e., vacuum pressure) was also observed at some regions for the cases of MC-AR, MC-SCR and MC-ACR. Thus, Fig. 6 is given here to provide the static pressure gradients for these cases. When fluid flow characteristics in these geometries are investigated more closely, secondary flow formations (i.e., fluid motion, which is perpendicular to the main flow direction.), vortices and recirculation zones can be observed. Briefly, the main flow velocity intensely decreased at the reentrant cavity zone due to the sudden expanded flow area [25]; furthermore, fluid entering into the cavity region was partially trapped and caused circulation regions. It was noted that the velocities within the cavity structure were much lower than the central portion of flow and the main flow pulled warmer fluid in the cavity to the central region. This resulted in laminar flow stagnation and pressure drop increment. This local circulation of flow is facilitated by mixing of colder water at the core flow and the warmer water near the channel wall [25].

Fig. 7 was also plotted to illustrate pressure variation, more specifically negative pressure with velocity vectors in more detail at the cavity region. When the flow velocity decreases anywhere in a channel, the static pressure increases at those regions; therefore, it is reasonable to observe negative pressures at these zones of the channel.

Fig. 8 (a) and Fig. 8 (b) show the formation of vortex in MC-SCR and the vortex bubble occurring after last cavity in MC-SCR, respectively. Pressure variation in the channel can sometimes cause separate flow regions indicated by the dashed line as shown in Fig. 8 (b). This separated flow, which can provide extra advantage in terms of heat transfer as pointed out by Zheng et al. [7], appears just after the final cavity for each case at different sizes. Moreover, the recirculation zones, which have a negative effect on heat transfer, are seen at the some locations. While positive pressure in the central region is observed, negative pressure values are seen in the cavity regions. The detailed effect of secondary flow and recirculation on thermal performance is going to be investigated with temperature outcomes in detail in the following sections. Lastly, boundary layer break up occurs when the flow separates from the leading edge of cavity and chaotic mixing discussed by Refs. [17] and [25] causes heat transfer improvement.

In addition to separated flow regions, previous studies discuss that longitudinal vortices can enhance the global heat transfer coefficient of a channel since these vortices nearly sweep the entire channel length while transverse vortices can only augment the local heat transfer coefficient of a channel [37]. Furthermore, based on a numerical analysis it was also reported that the presence of more multi-longitudinal vortices in the tube yields to more remarkable turbulent heat transfer enhancement for the tube side [38]. The longitudinal vortex heat transfer enhancement technology can improve the convection of the heat transfer performance effectively and is defined as the third-generation heat transfer technology [39]. For example, Fig. 9 and Fig. 10

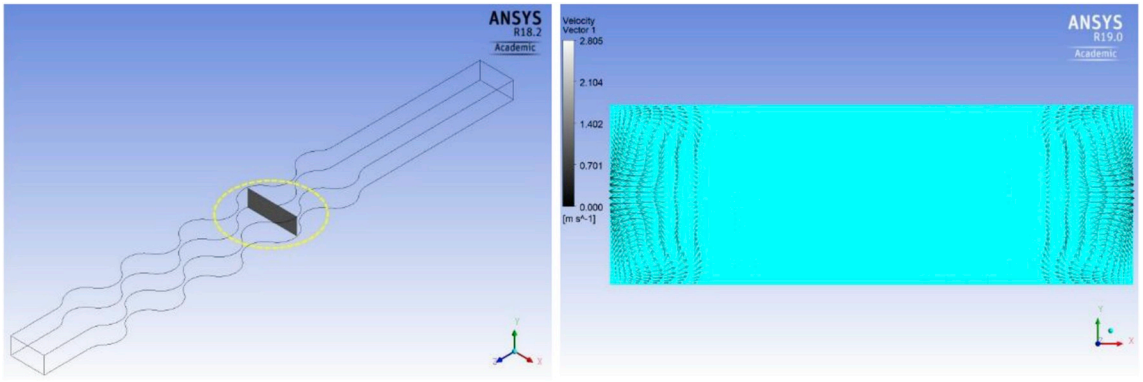

Fig. 9. The forming of longitudinal vortices in the MC-SCR (7.3 mm away from the inlet).

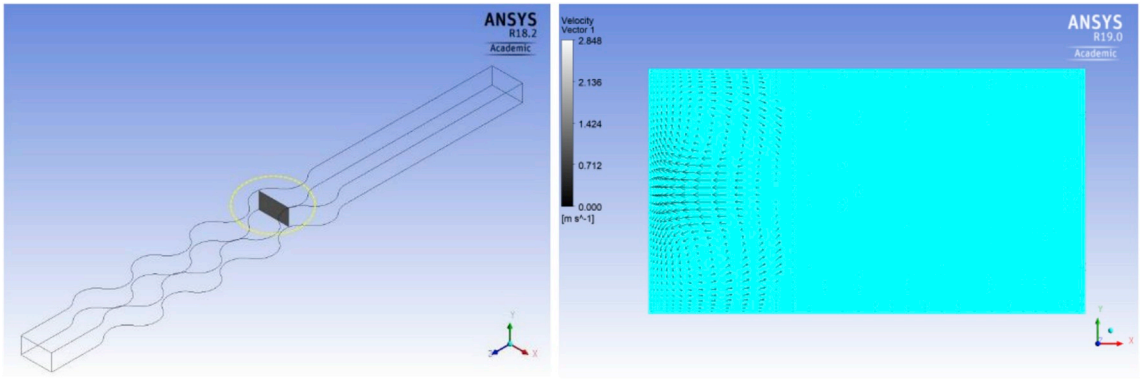

Fig. 10. The forming of longitudinal vortices in the MC-ACR (7.3 mm away from the inlet).

demonstrate the presence of longitudinal vortices for the case of MC-SCR and MC-ACR; therefore, the highest heat transfer is predicted for these cases. These figures show the x-y section areas of the MC-SCR and MC-ACR (i.e., perpendicular to the flow direction), which are nearly 7.3 mm away from the channel inlet as marked with yellow regions. It is also noted that the MC-SCR possesses vortices at each side due to the existence of two mutual cavities while the MC-ACR holds only one side since there is a cavity and a rib mutually for this case. Lastly, Meng et al. [38] reported that these types of vortices improve the temperature distribution along the microchannel although this finding was not exactly obtained in the scope of the present study.

4.2. Heat transfer characteristics

The baseline wall of a cooling plate works as an interface between a cooling plate and a device and this region is one of the most important part for electromechanical devices because temperature variation in these devices can directly affect the performance of the device and even can shorten the life of these devices. Therefore, it is required to have temperature uniformity on the wall as much as possible. Furthermore, temperature picks on the wall are not allowed since this can cause thermal runaway and eventually undermine the device's lifespan.

Fig. 11 illustrates temperature variation of the baseline walls (i.e., heated walls) for the entire cases. It was observed that temperature uniformity is directly affected by the positions of the cavities in the channel. When the cavities are placed asymmetrical, the main flow is directed in such a way that flow follows a path sweeping most of the baseline wall. This causes a small temperature gradient for the baseline wall in the studied cases. Furthermore, when the cross-sectional area of the microchannel gets smaller, the main flow is accelerated at those regions (i.e., out of the cavities) to satisfy conservation of mass. Therefore, well-mixed hot and cold fluids can be observed at accelerated flow regions. This can be seen as an improvement of flow disturbance since these regions provide low temperature values and similar findings were also discussed by Zheng et al. [13]. They also pointed out that optimum interaction of ribs and cavities in the channels enhances heat transfer significantly. On the other hand, 5–6 K temperature variation was observed in the last cavity of MC-SCR since the cavity pattern of this case traps the fluid flow causing a vortex bubble as seen in the red dash enclosed area of Fig. 8 (b). The trapped flow in this region could not be removed or carried with the main flow causing the existence of low velocity regions results in higher temperatures at these locations.

Another important parameter is the temperature distribution at the heated bottom wall because a more uniform temperature distribution on the interface wall ensures a prolonged lifespan of electronic device [40]. Table 3 shows the uniformity of temperature distribution on the baseline. According to the results shown in Table 3, the MC-AC is the best design depending on the maximum temperature rise of ΔT_b while the MC-SCR is the worst.

It is also noted that although the flow is assumed to be laminar, vortices are formed because of flow separation in the flow domain. However, this forming vortex and fluid flow is totally laminar since there is not any fluctuation in velocity, pressure or temperature profiles in the solution domain. On the other hand, while both thermal and hydrodynamics entrance lengths play a significant role in heat transfer analysis of microchannels, the present study findings stay in developing flow region for both thermally and hydrodynamically.

4.3. Performance evaluation

The most important requirements in microelectronic cooling applications are high heat transfer rate, low pressure drop and temperature uniformity at the contact region between device and cooling plate. Therefore, these concerns are needed to be considered altogether to design reliable and efficient micro-cooling equipment. In this part of the study, heat transfer enhancement factor, Nu_e/Nu_o, pressure drop penalty factor, f_e/f_o, and overall performance factor, ξ (as specified in Eq. (14)), for each simulated case at Reynolds number of 600 were evaluated and presented in Fig. 12.

Specifically, Fig. 12 (a) shows heat transfer enhancement values of MC-NCR, MC-AC, MC-AR, MC-SCR and MC-ACR cases. As the MC-SCR shows the best heat transfer performance, the MC-NCR has a poor heat transfer rate as expected. It is noted that the existence of symmetric cavity and ribs orient the flow in such a way that flow mixing causes augmentation in heat transfer. When the pressure drop is considered, the MC-ACR generates much more pressure drop compared to other cases as shown in Fig. 12 (b). The reason is the intense effect of recirculation and secondary flows as observed at the some channel locations. On the other hand, if both heat transfer and pressure drop characteristics are taken into account together, it is seen that the overall performance for the MC-AC, MC-AR and MC-SCR are more superior than the MC-NCR case. The overall performances are evaluated to be 8.54%, 6.25% and 0.17% for cases MC-SCR, MC-AC, and MC-AR, respectively. The interesting point is that the high pressure drop results in a significant decrease in overall performance; therefore, the MC-SCR illustrates the best channel design in terms of overall performance.

Geometric models: (a) a microchannel with no cavity and rib (MC-NCR); (b) a microchannel with asymmetric cavity (MC-AC) (c) a microchannel with asymmetric rib (MC-AR) (d) a microchannel with symmetric cavity and rib (MC-SCR) (e) a microchannel with asymmetric cavity and rib (MC-ACR).

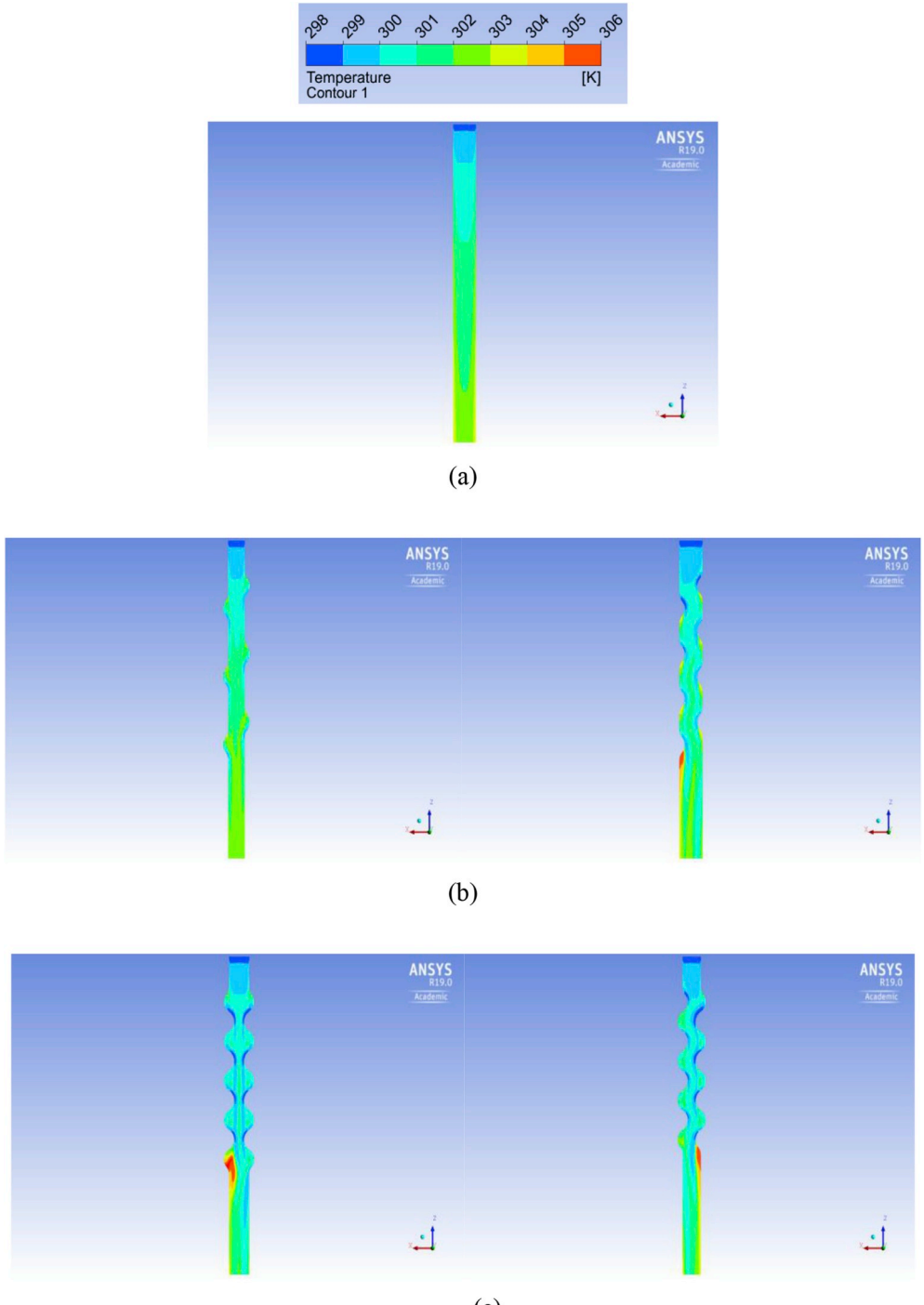

Fig. 11. The temperature distribution of baseline wall (heated wall) (a) MC-NCR (b) MC-AC and MC-AR (c) MC-SCR and MC-ACR.

Table 3
Uniformity of temperature distribution on the baseline.

Case	*Tmin*	*Tmax*	ΔT_b
MC-NCR	298.317	303.749	5.432
MC-AC	298.318	303.500	5.182
MC-AR	298.318	305.707	7.389
MC-SCR	298.321	306.931	8.610
MC-ACR	298.321	305.909	7.588

5. Conclusion

The effect of surface modification on thermal-hydraulic performance of the microchannel heat sinks (MCHS) was numerically investigated in detail under constant Reynolds number. The heat transfer, pressure drop, overall performance and temperature uniformity on baseline was also evaluated. The main conclusions extracted from this study are as follows:

1. The case of MC-SCR is the best in terms of heat transfer and overall performance through the positive effect of the combination of cavity

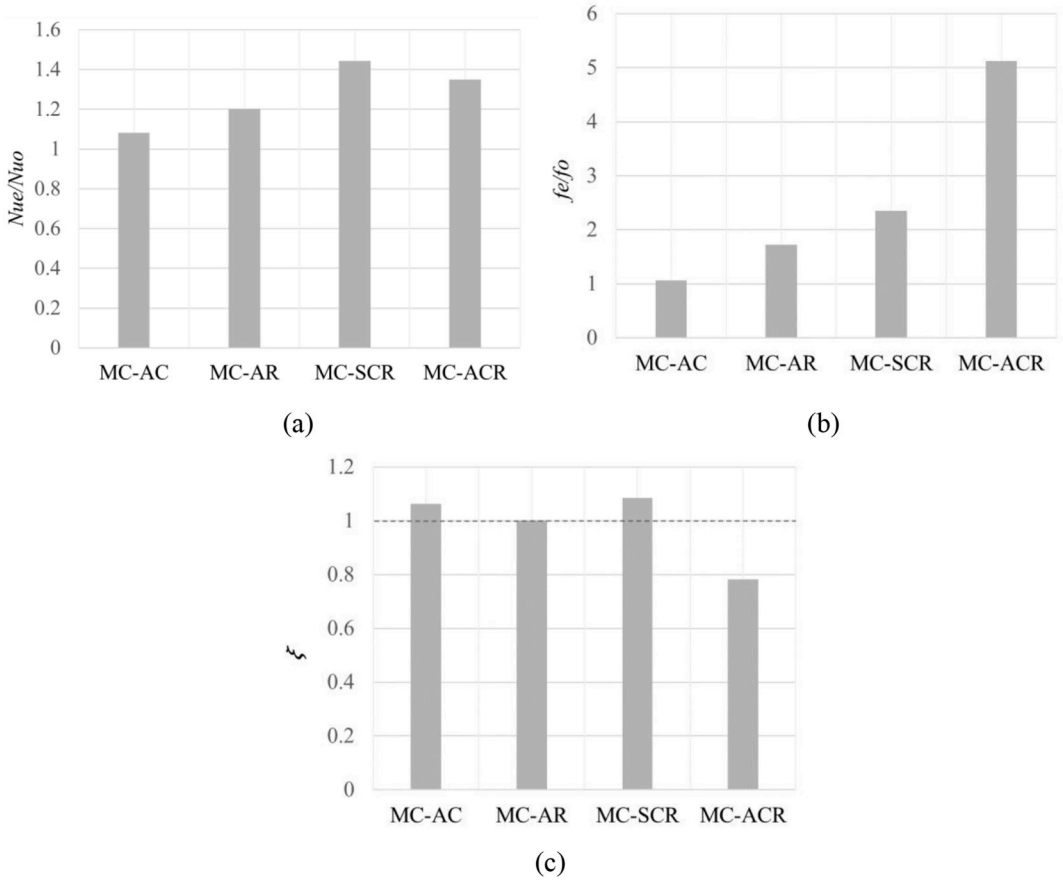

Fig. 12. Thermal-hydraulic performance for entire case (Re = 600) (a) heat transfer enhancement (b) pressure drop penalty (c) overall performance.

and rib. In addition, the vortices belonging to MC-SCR are considerably seen at both longitudinal and transverse axis and the jetting and throttling effect is dominant for this case when compared to other cases. The overall performance is followed the MC-AC, MC-AR, MC-NCR and MC-ACR, in descending order.

2. The best temperature uniformity on the baseline wall has been detected for MC-AC and the related case is about 40% better when compared to MC-SCR.
3. Although the case of MC-ACR is close to MC-SCR in terms of heat transfer, the overall performance is the worst one, even lower than MC-NCR because the recirculation zones are rather intensive in the cavities and they result in high pressure drop.
4. Vortices forming in cavity are an important phenomena for increasing heat transfer because they ensure a beneficial mixing between cold and hot water streams. However, an unsuitable cavity design can result in the increase of recirculation zones impeding heat transfer between near walls and core flow and cause pick temperature regions at local regions.
5. The temperature increase is observed intensively at the case of MC-AR, MC-SCR and MC-ACR since the cavity pattern of this case traps the fluid flow causing a vortex bubble. As similar to recirculation zone in cavity, the trapped flow in this region could not be removed or carried with the main flow causing existence of low velocity regions resulting in higher temperatures at these locations.

Acknowledgements

This work is partially supported by Scientific and Technological Research Council of Turkey (TÜBİTAK), Grant No: 114M774.

Appendix A. Supplementary data

Supplementary data to this article can be found online at https://doi.org/10.1016/j.ijthermalsci.2018.08.030.

References

[1] I.A. Ghani, N.A.C. Sidik, N. Kamaruzaman, Hydrothermal performance of microchannel heat sink: the effect of channel design, Int. J. Heat Mass Tran. (2017), https://doi.org/10.1016/j.ijheatmasstransfer.2016.11.031.
[2] N.M. Noh, A. Fazeli, N.A. Che Sidik, Numerical simulation of nanofluids for cooling efficiency in microchannel heat sink, J. Adv. Res. Fluid Mech. Therm. Sci. 4 (1) (2014) 13–23.
[3] R. Filimonov, J. Sorvari, Numerical study on the effect of cross-section orientation on fluid flow and heat transfer in a periodic serpentine triangular microchannel, Appl. Therm. Eng. (2017), https://doi.org/10.1016/j.applthermaleng.2017.07.027.
[4] Z. Wan, Q. Lin, X. Wang, Y. Tang, Flow characteristics and heat transfer performance of half-corrugated microchannels, Appl. Therm. Eng. (2017), https://doi.org/10.1016/j.applthermaleng.2017.05.176.
[5] M. Khoshvaght-Aliabadi, M. Sahamiyan, M. Hesampour, O. Sartipzadeh, Experimental study on cooling performance of sinusoidal-wavy minichannel heat sink, Appl. Therm. Eng. 92 (2016) 50–61, https://doi.org/10.1016/j.applthermaleng.2015.09.015.
[6] M. Khoshvaght-Aliabadi, F. Nozan, Water cooled corrugated minichannel heat sink for electronic devices: effect of corrugation shape, Int. Commun. Heat Mass Tran. 76 (2016) 188–196, https://doi.org/10.1016/j.icheatmasstransfer.2016.05.021.
[7] Z. Zheng, D.F. Fletcher, B.S. Haynes, Transient laminar heat transfer simulations in periodic zigzag channels, Int. J. Heat Mass Tran. 71 (2014) 758–768, https://doi.org/10.1016/j.ijheatmasstransfer.2013.12.056.
[8] Z. Dai, Z. Zheng, D.F. Fletcher, B.S. Haynes, Experimental study of transient behaviour of laminar flow in zigzag semi-circular microchannels, Exp. Therm. Fluid Sci. 68 (2015) 644–651, https://doi.org/10.1016/j.expthermflusci.2015.07.001.
[9] J. Rostami, A. Abbassi, M. Saffar-Avval, Optimization of conjugate heat transfer in wavy walls microchannels, Appl. Therm. Eng. 82 (2015) 318–328, https://doi.org/10.1016/j.applthermaleng.2015.02.069.
[10] D.D. Ma, G.D. Xia, Y.F. Li, Y.T. Jia, J. Wang, Effects of structural parameters on fluid flow and heat transfer characteristics in microchannel with offset zigzag grooves in sidewall, Int. J. Heat Mass Tran. 101 (2016) 427–435, https://doi.org/10.1016/j.

ijheatmasstransfer.2016.04.091.
[11] G. Lu, J. Zhao, L. Lin, X.D. Wang, W.M. Yan, A new scheme for reducing pressure drop and thermal resistance simultaneously in microchannel heat sinks with wavy porous fins, Int. J. Heat Mass Tran. 111 (2017) 1071–1078, https://doi.org/10.1016/j.ijheatmasstransfer.2017.04.086.
[12] L. Lin, J. Zhao, G. Lu, X.D. Wang, W.M. Yan, Heat transfer enhancement in microchannel heat sink by wavy channel with changing wavelength/amplitude, Int. J. Therm. Sci. 118 (2017) 423–434, https://doi.org/10.1016/j.ijthermalsci.2017.05.013.
[13] Z. Zheng, D.F. Fletcher, B.S. Haynes, Transient laminar heat transfer simulations in periodic zigzag channels, Int. J. Heat Mass Tran. 71 (2014) 758–768, https://doi.org/10.1016/j.ijheatmasstransfer.2013.12.056.
[14] M. Xu, H. Lu, L. Gong, J.C. Chai, X. Duan, Parametric numerical study of the flow and heat transfer in microchannel with dimples, Int. Commun. Heat Mass Tran. 76 (2016) 348–357, https://doi.org/10.1016/j.icheatmasstransfer.2016.06.002.
[15] G. Xia, D. Ma, Y. Zhai, Y. Li, R. Liu, M. Du, Experimental and numerical study of fluid flow and heat transfer characteristics in microchannel heat sink with complex structure, Energy Convers. Manag. 105 (2015) 848–857, https://doi.org/10.1016/j.enconman.2015.08.042.
[16] H.E. Ahmed, M.I. Ahmed, Optimum thermal design of triangular, trapezoidal and rectangular grooved microchannel heat sinks, Int. Commun. Heat Mass Tran. 66 (2015) 47–57, https://doi.org/10.1016/j.icheatmasstransfer.2015.05.009.
[17] L. Chai, G. Xia, M. Zhou, J. Li, Numerical simulation of fluid flow and heat transfer in a microchannel heat sink with offset fan-shaped reentrant cavities in sidewall, Int. Commun. Heat Mass Tran. 38 (2011) 577–584, https://doi.org/10.1016/j.icheatmasstransfer.2010.12.037.
[18] N. Zheng, P. Liu, Z. Liu, W. Liu, Numerical simulation and sensitivity analysis of heat transfer enhancement in a flat heat exchanger tube with discrete inclined ribs, Int. J. Heat Mass Tran. (2017), https://doi.org/10.1016/j.ijheatmasstransfer.2017.05.019.
[19] G. Xia, Z. Chen, L. Cheng, D. Ma, Y. Zhai, Y. Yang, Micro-PIV visualization and numerical simulation of flow and heat transfer in three micro pin-fin heat sinks, Int. J. Therm. Sci. (2017), https://doi.org/10.1016/j.ijthermalsci.2017.05.015.
[20] C. Chen, J.T. Teng, C.H. Cheng, S. Jin, S. Huang, C. Liu, M.T. Lee, H.H. Pan, R. Greif, A study on fluid flow and heat transfer in rectangular microchannels with various longitudinal vortex generators, Int. J. Heat Mass Tran. 69 (2014) 203–214, https://doi.org/10.1016/j.ijheatmasstransfer.2013.10.018.
[21] I.A. Ghani, N. Kamaruzaman, N.A.C. Sidik, Heat transfer augmentation in a microchannel heat sink with sinusoidal cavities and rectangular ribs, Int. J. Heat Mass Tran. (2017), https://doi.org/10.1016/j.ijheatmasstransfer.2017.01.046.
[22] X. Huang, W. Yang, T. Ming, W. Shen, X. Yu, Heat transfer enhancement on a microchannel heat sink with impinging jets and dimples, Int. J. Heat Mass Tran. (2017), https://doi.org/10.1016/j.ijheatmasstransfer.2017.04.078.
[23] Y.F. Li, G.D. Xia, D.D. Ma, Y.T. Jia, J. Wang, Characteristics of laminar flow and heat transfer in microchannel heat sink with triangular cavities and rectangular ribs, Int. J. Heat Mass Tran. 98 (2016) 17–28, https://doi.org/10.1016/j.ijheatmasstransfer.2016.03.022.
[24] Y. Zhai, G. Xia, Z. Chen, Z. Li, Micro-PIV study of flow and the formation of vortex in micro heat sinks with cavities and ribs, Int. J. Heat Mass Tran. 98 (2016) 380–389, https://doi.org/10.1016/j.ijheatmasstransfer.2016.03.044.
[25] G. Xia, Y. Zhai, Z. Cui, Numerical investigation of thermal enhancement in a micro heat sink with fan-shaped reentrant cavities and internal ribs, Appl. Therm. Eng. 58 (2013) 52–60, https://doi.org/10.1016/j.applthermaleng.2013.04.005.
[26] G.D. Xia, J. Jiang, J. Wang, Y.L. Zhai, D.D. Ma, Effects of different geometric structures on fluid flow and heat transfer performance in microchannel heat sinks, Int. J. Heat Mass Tran. 80 (2015) 439–447, https://doi.org/10.1016/j.ijheatmasstransfer.2014.08.095.
[27] I.A. Ghani, N.A.C. Sidik, R. Mamat, G. Najafi, T.L. Ken, Y. Asako, W.M.A.A. Japar, Heat transfer enhancement in microchannel heat sink using hybrid technique of ribs and secondary channels, Int. J. Heat Mass Tran. (2017), https://doi.org/10.1016/j.ijheatmasstransfer.2017.06.103.
[28] N. Raja Kuppusamy, R. Saidur, N.N.N. Ghazali, H.A. Mohammed, Numerical study of thermal enhancement in micro channel heat sink with secondary flow, Int. J. Heat Mass Tran. 78 (2014) 216–223, https://doi.org/10.1016/j.ijheatmasstransfer.2014.06.072.
[29] M.E. Steinke, S.G. Kandlikar, Single-Phase liquid heat transfer in plain and enhanced microchannels, ASME 4th Int. Conf. Nanochannels, Microchannels, Minichannels, Parts A B. 2006 (2006) 943–951, https://doi.org/10.1115/ICNMM2006-96227.
[30] X. Yu, C. Woodcock, J. Plawsky, Y. Peles, An investigation of convective heat transfer in microchannel with Piranha Pin Fin, Int. J. Heat Mass Tran. 103 (2016) 1125–1132, https://doi.org/10.1016/j.ijheatmasstransfer.2016.07.069.
[31] X. Wang, B. An, J. Xu, Optimal geometric structure for nanofluid-cooled microchannel heat sink under various constraint conditions, Energy Convers. Manag. 65 (2013) 528–538, https://doi.org/10.1016/j.enconman.2012.08.018.
[32] L. Lin, Y.Y. Chen, X.X. Zhang, X.D. Wang, Optimization of geometry and flow rate distribution for double-layer microchannel heat sink, Int. J. Therm. Sci. 78 (2014) 158–168, https://doi.org/10.1016/j.ijthermalsci.2013.12.009.
[33] C. Leng, X. Wang, T. Wang, An improved design of double-layered microchannel heat sink with truncated top channels, Appl. Therm. Eng. 79 (2015) 54–62, https://doi.org/10.1016/j.applthermaleng.2015.01.015.
[34] M.E. Steinke, S.G. Kandlikar, Single-phase liquid friction factors in microchannels, Int. J. Therm. Sci. 45 (2006) 1073–1083, https://doi.org/10.1016/j.ijthermalsci.2006.01.016.
[35] R.L. Webb, Performance evaluation criteria for use of enhanced heat transfer surfaces in heat exchanger design, Int. J. Heat Mass Tran. 24 (1981) 715–726, https://doi.org/10.1016/0017-9310(81)90015-6.
[36] J.M. Wu, J.Y. Zhao, K.J. Tseng, Parametric study on the performance of double-layered microchannels heat sink, Energy Convers. Manag. 80 (2014) 550–560, https://doi.org/10.1016/j.enconman.2014.01.014.
[37] J.M. Wu, W.Q. Tao, Numerical study on laminar convection heat transfer in a rectangular channel with longitudinal vortex generator. Part A: verification of field synergy principle, Int. J. Heat Mass Tran. 51 (2008) 1179–1191, https://doi.org/10.1016/j.ijheatmasstransfer.2007.03.032.
[38] J.A. Meng, X.G. Liang, Z.X. Li, Field synergy optimization and enhanced heat transfer by multi-longitudinal vortexes flow in tube, Int. J. Heat Mass Tran. 48 (2005) 3331–3337, https://doi.org/10.1016/j.ijheatmasstransfer.2005.02.035.
[39] A.E. Bergles, ExHFT for fourth generation heat transfer technology, Exp. Therm. Fluid Sci. 26 (2002) 335–344, https://doi.org/10.1016/S0894-1777(02)00145-0.
[40] Y. Zhai, Z. Li, H. Wang, J. Xu, Thermodynamic analysis of the effect of channel geometry on heat transfer in double-layered microchannel heat sinks, Energy Convers. Manag. (2017), https://doi.org/10.1016/j.enconman.2017.04.013.